LA-UR-99-870

FORTE observations of lightning radio-frequency signatures: Prompt coincidence with strokes detected by the National Lightning Detection Network

Abram R. Jacobson[1]

Kenneth L. Cummins[2]

Michael Carter[1]

Phillip Klingner[1]

Diane Roussel-Dupré[1]

Stephen O. Knox[1]

[1]Los Alamos National Laboratory [2]Global Atmospherics, Inc.

Abstract

This work compares contemporaneous observations of lightning from two highly complementary systems. FORTE is a low-Earth-orbit satellite carrying radio-wave and optical instruments for the study of lightning. The radio receivers aboard FORTE observe very-high-frequency (VHF) emissions from the air-breakdown process preceding and (sometimes) accompanying large-scale current flow. Only VHF (and higher) emissions from lightning can reliably penetrate the ionosphere to a satellite, especially along grazing-incidence paths. The National Lightning Detection Network (NLDN) is a ground-based array of sensors in the continental United States (CONUS) observing the low-frequency (LF) and very-low-frequency (VLF) radiation from large-scale vertical currents. Prior to the launch of FORTE in 1997, essentially no work had been done on the statistical correlations between (a) ground-based LF/VLF and (b) spaced-based VHF remote sensing of lightning. During April – September 1998, FORTE was tasked with taking maximum triggered VHF data over and near the CONUS, and NLDN data was specially post-processed in a loosened-criterion mode providing enhanced detection range beyond the CONUS. The time history of reported events from the two systems was compared, and event pairs (each pair containing one event from FORTE, the other from NLDN) that were candidate correlations (closer than 200 ms from each other) were scrutinized to determine if there was a statistically meaningful timing relationship. We have found that there is a statistically significant correlation , consisting of a prompt coincidence between a subset of NLDN events and a subset of FORTE events. This coincidence is most likely to occur for intracloud, and less likely to occur for cloud-to-ground discharges. The prompt coincidences mostly are within ±50 μs, after correction for the propagation of the VHF signal to FORTE from the NLDN-geolocated discharge. The NLDN-furnished geolocation of the prompt-coincident FORTE-observed VHF pulses allows the pulses to be better

interpreted. In particular, we can deduce, from the lag of the VHF ground-reflection echo, the height of the VHF emission region in the storm.

1. Introduction and background

Thunderstorms are known to emit very-high-frequency (VHF; 30 - 300 MHz) pulses, which researchers have learned to associate with the air-breakdown process [*Hayenga and Warwick*, 1981; *Le Vine*, 1980; *Proctor*, 1981; *Proctor et al.*, 1988; *Rhodes et al.*, 1994; *Shao et al.*, 1996; *Shao and Krehbiel*, 1996; *Smith and Holden*, 1996; *Smith et al.*, 1998; *Weidman and Krider*, 1979; *Willett et al.*, 1989]. These workers also studied a very complex and varied interrelationship between the LF/VLF ("sferic") and VHF discharge signatures during the development and decay of the lightning flash. Furthermore, VHF pulses emitted by the storm have been found to be either "major", that is, in a set of pulses grouped in time according to flashes and associated with LF/VLF signatures, or "minor", occurring higher in altitude and less obviously related to LF/VLF signatures or indeed to other "minor" VHF pulses [*Taylor et al.*, 1984].

Relatively less scientific information about lightning VHF emissions has been forthcoming from sensors aboard satellites. The Blackbeard VHF receiver system aboard the ALEXIS satellite [*Holden et al.*, 1995; *Massey and Holden*, 1995; *Massey et al.*, 1998] provided for the first time a space-based scientific transient-waveform recorder's view of lightning VHF on a global scale. Blackbeard observed almost exclusively a very high-energy, narrow-pulse VHF emission, which occured in a pair, was ionospherically dispersed, and came to be known as a "transionospheric pulse pair", or TIPP. Although the Blackbeard data were somewhat consistent with a ground-reflection model for the second pulse [*Massey and Holden*, 1995], there were other models, including one involving an upward discharge propagating into the mesosphere [*Roussel-Dupré and Gurevich*, 1996].

Blackbeard collected very few TIPPs that could be ground-truthed with other measurements, although the few exceptions have been well analyzed and reported upon [*Zuelsdorf et al.*, 1998; *Zuelsdorf et al.*, 1997].

The FORTE satellite (Fast On-Orbit Recording of Transient Events) was launched on 29 August 1997, and carried a VHF receiver system representing significant improvements over Blackbeard. Initial FORTE observations of VHF lightning emissions revealed both Blackbeard-like TIPPs and weaker, longer-duration emissions [*Jacobson et al.*, 1999]. The case was strengthened for a ground-reflection explanation of TIPPs. In addition, since a single satellite cannot determine the location of a VHF emission (other than to constrain that emission to lie within the small circle representing the Earth's limb seen from the satellite), there developed an interest in geolocating emission centers associated with VHF signals seen by FORTE. This would allow an important advance in converting satellite datastreams into useful and quantitative information about radio emissions from lightning. Such information would include the absolute power and energy at the storm-located source of the VHF emission, as well as the height of the TIPP emission by interpreting the interpulse separation [*Jacobson et al.*, 1999].

In order to do this, we sought to rely on the association of at least some of the detected VHF emissions with LF/VLF signatures of lightning discharges. The National Lightning Detection Network (NLDN) comprises broadband sensors covering the LF/VLF band and routinely monitors the CONUS and surrounding areas, detecting and geolocating (at >80% efficiency) cloud-to-ground vertical currents of sufficient magnitude (>5 kA), and also detects and geolocates some intracloud discharges [*Cummins et al.*, 1998; *Idone et al.*, 1998a; *Idone et al.*, 1998b]. The strategy we adopted was to seek statistically significant coincidences between NLDN-detected discharges and FORTE VHF timestamps, and then to assign the source discharge geolocation (latitude, longitude) to the VHF emission

source. We did not know at the outset *how many* FORTE VHF events over the NLDN area should be expected to have an accompanying LF/VLF signature detectable by NLDN. Earlier published Blackbeard/NLDN comparitive studies [*Zuelsdorf et al.*, 1998; *Zuelsdorf et al*., 1997] had inferred that TIPPs are mostly associated with intracloud processes, and therefore unlikely to occur in close coincidence with NLDN strokes (which are mostly cloud-to ground). This will turn out to be largely confirmed in the present work.

2. The FORTE rf system

2. (a) General capabilities

The FORTE satellite has performed continuous observations of lightning since its launch on 29 August 1997. FORTE is in a 70° inclination, circular low-Earth orbit and makes several passes per day over lightning-prone tropical regions, notably South America, Africa, and SE Asia/ Indonesia, as well as over the less lightning-prone midlatitudes. FORTE captures and stores discrete records of VHF lightning signatures. The radio-frequency (rf) receiver comprises two 50-Megasample-per-second passbands, each analog-filtered to 22-MHz bandwidth. In the data to follow, we typically run with (at least) one 22-MHz channel placed in the range 26-48 MHz, with a nominal 38-MHz center ("low band"), and the other in the range 118 - 140 MHz, with a nominal 130-MHz center ("high-band"). This allows the VHF signal spectrum to be roughly inferred from the relative power on the two channels. The low-band trigger was used in this work. Low-band triggering was used because it tends to trigger on the more intense part of the signal spectrum [*Jacobson et al.*, 1999]. The performance of the FORTE rf payload, plus some of the initial characteristics of the lightning observations, have been described in detail elsewhere [*Jacobson et al.*, 1999].

There are eight "trigger subbands" in each 22-MHz-wide receiver channel. Each 1-MHz-wide trigger subband has a noise-compensation option, so that the trigger threshhold is

either set in absolute level or as dB *above a low-pass-filtered noise level* in that 1-MHz subband, i.e. as a "noise-riding threshold". In this way the trigger system can in practice trigger on lightning signatures that would otherwise be overwhelmed by anthropogenic radio carriers appearing in the overall analog passband. In the data used here, we use noise-riding-threshhold triggering and require five (out of eight) 1-MHz subbands to trigger in coincidence (with a coincidence window adequate to compensate for ionospheric dispersion, namely 162 μs). We typically require the signal to transiently rise at least 14 - 20 dB (depending on the program and the intended class of lightning signals) above the noise background in each 1-MHz subband contributor to the "5-out-of-8" OR condition. These contributing channels must arrive within a coincidence time of 162 μs of each other. This allows for ionospheric dispersion of the pulse.

Both 22-MHz channels are connected to different linear polarizations of a two-polarization log-periodic antenna. The antenna is mounted on a boom facing the satellite nadir, usually within a few degrees. The antenna is designed to place an approximate minimum (througout the VHF spectrum) on the limb of the Earth as seen from FORTE, and a lobe maximum at nadir. From orbital altitude, the limb is located on a “small circle” of arc-diameter 6,400 km.

The Data Acquisition System (DAS) contains enough memory for up to 0.8 seconds (cumulative) of 12-bit data simultaneously from the two 22-MHz channels. Each record is triggered (see above) and has adjustable pre/post-trigger ratio. We typically use 400- μs records with 100 μs of pretrigger samples and 300 μs of posttrigger samples. There is typically room in DAS memory for ~2000 such events between downloads. Since we can have up to several downloads per day, in principle we can acquire up to ~10000 such events per day. Usually, however, operations constraints and availability of suitable storms near the FORTE track limit us to less than this theoretical maximum.

The DAS is capable of beginning a new record 162 μs after the end of the previous record, so that FORTE records can effectively mosaic-together to form a quasi-continuous registation of VHF signatures arriving one-upon-the-other within a flash. We find in practice that the registration of records is not impeded by the necessary DAS dead time between records, but rather is spaced wider apart by the cadence of the emission process itself [*Jacobson et al.*, 1999].

2. (b) Typical rf data and triggering biases

It is important to realize that observations of lightning VHF from space are intrinsically insensitive and perforce are limited to only the brightest lightning VHF emissions. The noise is in all but a few cases entirely due to the Earth scene noise, and is not imposed by the receiver. This is due to the tendency of a space-based sensor to collect anthropogenic and natural radio noise summed over the entire viewed area on Earth. For a distant satellite this viewed area is half the Earth. Even for FORTE, the anthropogenic noise can, in priniciple, derive from a huge contributory area, anywhere within a small circle of arc-radius 6400 km, although the nadir gain of the antenna vignettes this field of view somewhat. This contributory area comprises, for example, all of the continental United States when FORTE is over the Great Plains.

This radio-noise background forced FORTE's predecessor, the Blackbeard VHF receiver [*Holden et al.*, 1995; *Massey and Holden*, 1995] aboard the ALEXIS satellite, to limit its observations to the brightest radio emissions from lightning, "transionospheric pulse pairs" (TIPPs). Blackbeard triggered off a rectified, 1- μs average of the entire power in the passband. This all-band triggering scheme provided less protection from modulated-carrier noise than does the FORTE multiband-coincidence trigger. The TIPP pulses seen by

Blackbeard were estimated to originate in a typically 1-joule (isotropic) burst of energy in the VHF, happening in a few microseconds (or less), consistent with peak source powers up to10^6 Watts isotropic [*Massey and Holden*, 1995].

FORTE's multichannel-coincidence trigger results in an improved ability to see diffuse and weaker VHF emissions relative to Blackbeard, but nonetheless we are still limited to seeing only those VHF sources that are very intense compared to what can be observed with close-in, ground-based sensors. This is because the ground based sensors are shielded from distant noise by their nearby line-of-sight radio horizon.

Plate 1: Spectral density of electric field E (left column), and total E^2 versus time (right column) for a weak FORTE event at 21:10:10 UT on 3 January 1999. The time series are 410 μs long. Top panel: Raw data. Middle panel: postwhitened data. Bottom panel: postwhitened, dechirped data.

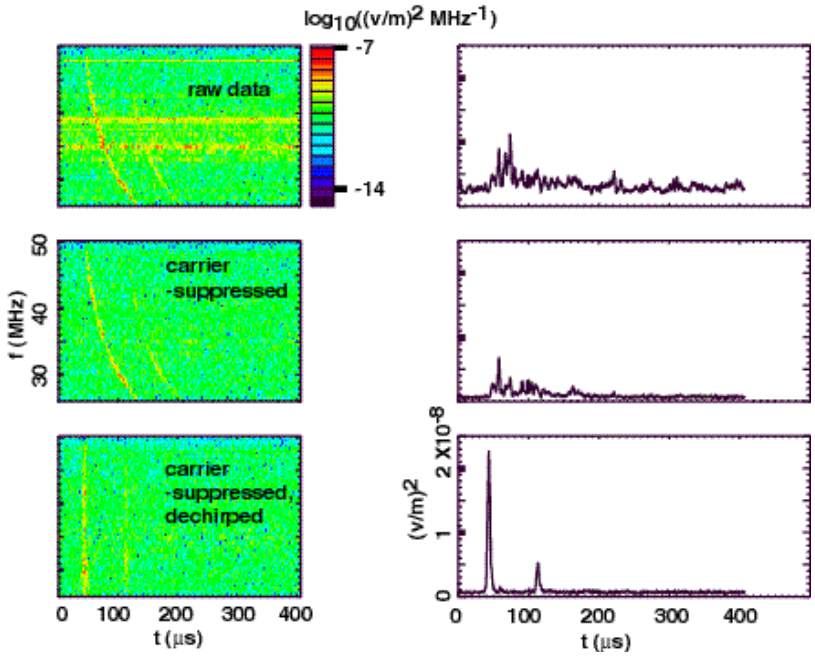

Plate 1 shows data from a typical "weak-event" (compared to Blackbeard, or even to the majority of FORTE events at three different stages of FORTE processing). This event represents the lower quartile of lightning VHF events seen by the FORTE receiver, in terms of power. The left column shows the logarithm (base 10) of the spectral density in periodogram format, with time running horizontally and frequency vertically.

The right column shows the time-history of the frequency-integrated spectral density, or the time-history of the instantaneous electric-field-squared in the 22-MHz band.

The top row in Plate 1 shows the "raw" data, from which the 5-out-of-8 trigger criterion is satisfied at ~100 μs into the record. The two chirped (dispersed) lightning signals are not much stronger than the background, as seen in the right panel; indeed, the signal-to-noise ratio (SNR) is only 3. Blackbeard in its normal configuration would not have triggered off such a weak lightning VHF event, for to have been so configured would have resulted in Blackbeard's having to accept many false events consisting of noise. The FORTE multichannel trigger criterion is satisfied by the first lightning pulse , with a 162- μs inter-channel coincidence window allowing the trigger subchannels to vote in lags varying ~$1/f^2$ due to pulse dispersion. The pulse is followed by a ground-reflection echo [*Jacobson et al.*, 1999]. The background is primarily due to partially modulated carriers, one near the top of the spectrum, and several in the middle of the spectrum.

The middle row in Plate 1 shows the "postwhitened" data, in which rows containing carriers are suppressed in proportion to the particular carrier's time-averaged intensity [*Jacobson et al.,* 1999]. The SNR is higher (~8). Finally, the bottom row in Plate 1 shows the dechirped data [*Jacobson et al.*, 1999], and now SNR>15. The pulse structure (primary pulse, plus ground reflection) is well-resolved in the electric-field-squared. The dechirping algorithm provides an estimate of the total electron content (TEC) along the slant path from the satellite to the emitter. The primary pulse's peak electric-field-squared is on the order of $2X10^{-8}$ $(V/m)^2$, corresponding to a power flux density of $5X10^{-11}$ Watts/m^2 at the satellite. A typical range from FORTE to an emission is 1000 - 3000 km. Assuming that the source is an isotropic radiator located 2000 km away (slant path) from the satellite, we infer a

source peak-emitted istropic power (in the 22-MHz bandwidth) of ~ 2.7 KW, or a power spectral density of ~10^2 Watts/MHz.

3. The NLDN array

The NLDN is described in detail elsewhere [*Cummins et al.*, 1998]. The NLDN is comprised of 59 LPATS-III Time-of-Arrival (TOA) sensors and 47 IMPACT sensors that provide both TOA and direction-finding information. These ground-based sensors transmit lightning data to a Network Control Center (NCC) in Tucson, Arizona, via a two-way satellite communication system. Data from the remote sensors are recorded and then processed in the NCC to provide the time, location, an estimate of the peak current, and other waveform and data-quality parameters for each detected cloud-to-ground lightning return stroke. The real-time data are then sent back out the communications network for satellite broadcast dissemination to real-time users. All this takes place within 30-40 seconds of each lightning flash. All recorded data are reprocessed off-line within a few days of acquisition and then stored in a permanent database that can be accessed by users who do not require real-time information. The median location accuracy provided by the NLDN is 500 meters, and the estimated flash detection efficiency varies between 80 and 90 percent, for peak currents greater then 5 kA [*Cummins et al.*, 1998; *Idone et al.*, 1998a; *Idone et al.*, 1998b].

The NLDN sensors are responsive to radiation field signals in the LF and VLF frequency ranges, and are thereby sensitive to ground-wave lightning return-stroke fields over a spatial range of about 30 to 650 km. They are also responsive to lightning-produced VLF fields that have been reflected by the ionosphere, and to a subset of fields produced by cloud discharges that emit significant energy in the LF frequency range. The IMPACT

sensors are designed to reject many of these cloud discharges and "reflected" signals, based on waveform criteria, but the LPATS-III sensors accept a broader range of waveshapes.

The standard NLDN lighting data are carefully quality controlled and limited to minimize mis-located "outlier" events, employing specific criteria [*Cummins et al.*, 1998]. For the purposes of this study, we reprocessed the raw sensor from the LPATS-III sensors employing relaxed criteria, in order to maximize the detection of both cloud discharges and distant CG discharges. Specifically, "unverified" locations produced by three LPATS-III (TOA) sensors were accepted, no maximum limit was set for the distance between a sensor and the discharge location, and a number of waveform-consistency criteria were relaxed to accommodate ionospherically propagated signals. The resulting dataset therefore included some very distant CG lighting discharges (sferics), occurring several thousand km outside the network, as well as very energetic cloud discharges occurring within or near the network. Given the relaxed criteria, the dataset also included numerous outliers. This did not pose a problem in the current study, since the lighting data was time-correlated with FORTE events with 10-μs resolution.

The located lightning discharges were classified as follows. Events for which all contributing sensors reported a narrow pulse-width, identified by a peak-to-zero time of less than 10 μs, were identified as cloud discharges. All other discharges were identified as cloud-to-ground. For those events in which the closest reporting sensor was more than 625 km from the calculated location, the estimated signal strength (peak current) was set to zero. This assignment reflects the uncertainty in the source strength when the ground wave becomes smaller than the ionospheric reflection.

Figure 1: Cartoon of joint FORTE/NLDN observationof the same storm. The FORTE satellite receives VHF pulses from an emission center above the ground, giving rise to the reception of a delayed echo caused by ground reflection. The FORTE data for a single event carries no information about where the emission center is located. However, if the emission latitude and longitude can be inferred by other means, then the emission height can be retrieved from the echo's delay (relative to the first pulse). The NLDN array detects the associated LF/VLF LF/VLF signature radiated horizontally from a large-scale, slow discharge current. If three or more NLDN stations detect the LF/VLF signature, then NLDN has the opportunity to geolocate the source. When that happens, the FORTE VHF timestamp can be compared to the NLDN stroke timestamp, after correction for VHF propagation delay.

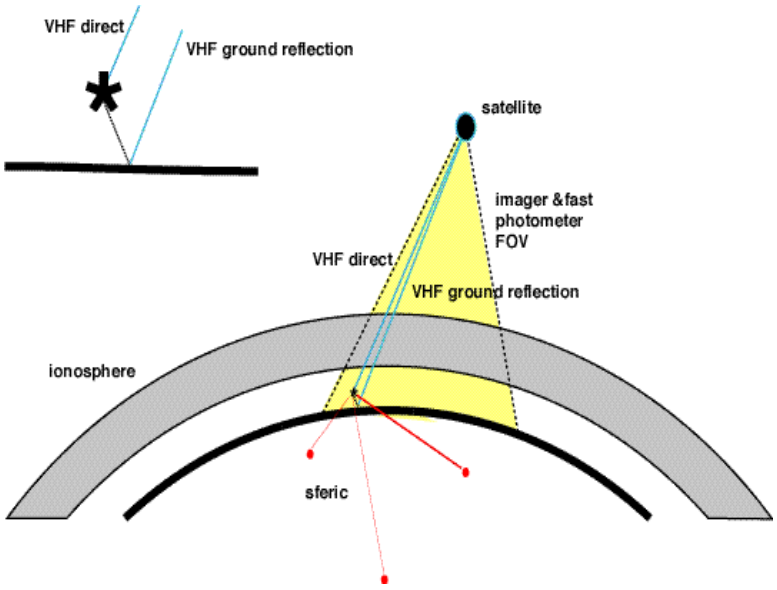

One additional behavior of the NLDN, following the 1995 upgrade, is salient to the work described here. The increase in NLDN sensitivity and changes to waveform acceptance criteria have generated a previously undetected population of small positive discharges. Specifically, it appears that a reduction in the minimum waveform width criterion in the IMPACT sensors, intended to allow detection of near-threshold signals, also allows the detection of a small fraction of the relatively large, long-duration isolated cloud pulses. We believe that these discharges are mis-classified as CG, since the IMPACT sensors also report them [*Cummins et al., 1998]*. Therefore, in portions of this study, we will caution that small positive CG discharges (estimated peak current less then 10 kA) may be a separate population (see below).

4. The joint FORTE-NLDN campaign

4. (a) Basic coincidence statistics

During April - September 1998, FORTE acquired events over the North American region whenever possible, typically in several passes per day, each pass lasting up to 20 minutes. The FORTE events are time-stamped with a GPS on-board timing and subsecond-counter system, to an accuracy on the order of 1 μs. The relaxed-criterion NLDN stroke reports had event time accuracies better than 10 μs (consistent with geolocation spatial accuracies better than 3 km), at least over the CONUS. This six-month campaign's FORTE and NLDN archives were compared to identify coincident events. Figure 1 is a cartoon showing a typical joint FORTE/NLDN detection. FORTE receives a lightning VHF pulse and, in principle, that pulse's ground reflection (see the second pulse in Plate 1). The VHF emission may be associated with LF/VLF emission, which is detected and geolocated/timed by NLDN. The VHF signal is postwhitened and de-chirped (see above), and the TEC is estimated from the optimal dechirp.

The added value of seeking FORTE coincidence with NLDN, rather than treating data from FORTE autonomously, is that NLDN can provide horizontal geolocations (latitude, longitude) and lightning-discharge characterization, ancillary information with which the FORTE VHF signals can be more meaningfully interpreted. The most obvious immediate advantage of this would be to infer the height (above the reflecting ground) of a VHF emission source [*Jacobson et al.*, 1999; *Smith*, 1998], using the latitude and longitude provided by a coincident-LF/VLF geolocation. As can be seen qualitatively in the Figure 1 cartoon, knowledge of the VHF source latitude and longitude allows calculation of the elevation angle of the satellite seen from the VHF source, and this allows retrieval of the source height [*Jacobson et al.*, 1999]. Another item of added value from geolocation is that we can correct the received VHF power and energy (at FORTE) for $1/r^2$ and thus infer the source power and energy irrespective of the emitter's distance from the subsatellite point.

In order to focus on candidate NLDN-FORTE coincidences, we now limit the discussion to FORTE events which are within ± 200 ms of an NLDN stroke. During the six-month campaign, this amounts to a quarter-million FORTE events. For this limited set, we correct the FORTE timestamp by subtracting from it the vacuum time-of-flight along the slant path to the putatively correlated NLDN LF/VLF signature. This correction makes up to >10 ms difference. In addition, we use an ellipsoidal geoid for the Earth's surface figure; this makes a correction of ~10 μs compared to using a spherical Earth approximation. Finally, we correct for the plasma contribution to the group delay, using the TEC retrieved from the optimal dechirp. This latter correction amounts to tens of μs, depending on TEC.

To show the basic behavior of this distribution, we begin in Figure 2 with a display of data for four individual passes of FORTE over the CONUS, each lasting several minutes. Each pass is represented by a histogram of LF/VLF-FORTE timestamp difference, from -20 ms to +20 ms, in 0.2-ms bins. Each pass shows a prominent and statistically significant central peak, corresponding to prompt coincidence (at least on a millisecond timescale) between the LF/VLF time and the corrected FORTE time. Each pass also shows vague suggestions of other, but less prompt, coincidences on either side of the central peak. One question is whether the latter are (a) in any sense reproducible from pass to pass, (b) reproducible throughout the campaign, or (c) peculiar to each pass and mutually random between passes.

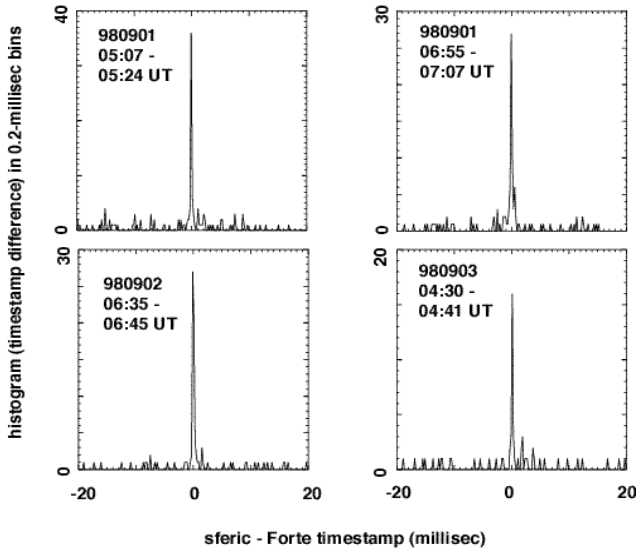

Figure 2: Histograms of difference of NLDN lightning discharge timestamp minus FORTÉ VHF timestamp,, during four representative FORTÉ passes over the CONUS region.

Figure 3 addresses this issue of reproduciblity, showing the campaign-totaled histogram of the quarter-million timestamp differences, from -0.2 sec to +0.2 sec, in 1-ms bins. The prompt coincidence is the *only coincidence feature* that is reproducible enough to survive this gross averaging over passes and months. The floor (at a level ~700 events per ms) is otherwise featureless; the floor outside the prompt peak is assumed to be due to accidental coincidence. We must assume that this floor underlies the prompt peak, too, so that if we stopped here, we would face an unacceptably large accidental-coincidence contamination of the central peak.

Figure 3: Histogram of difference of NLDN lightning discharge timestamp minus FORTÉ VHF timestamp, comprising all data taken in the six-month joint campaign. A 1-ms bin is used.

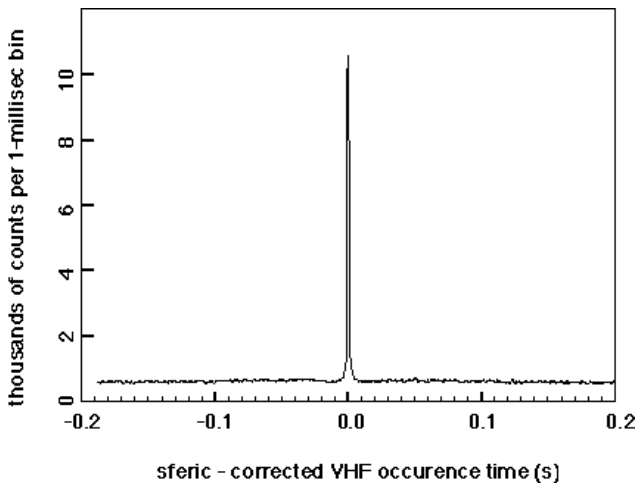

We saw in the per-pass coincidence histograms (Figure 2 above) that the central peak is probably narrower than the 1-ms bin used in Figure 3. Thus we explore a similar histogram for all the campaign data, but with a narrower bin size. This is shown in Figure 4, which runs only from -2 ms to +2 ms, and uses only a 10-μs bin size. This finer examination of the coincidence distribution reveals that the prompt peak is intrinsically less than 0.3 ms wide at half-max, that the peak:background ratio has now been improved to >100 (whereas the ratio had been ~14 in Figure 3), and that the peak appears to be bimodal, with a splitting of tens of μs.

Figure 4: Similar to Figure 3, but with a 10μ bin and zoomed-in to range ±2 ms.

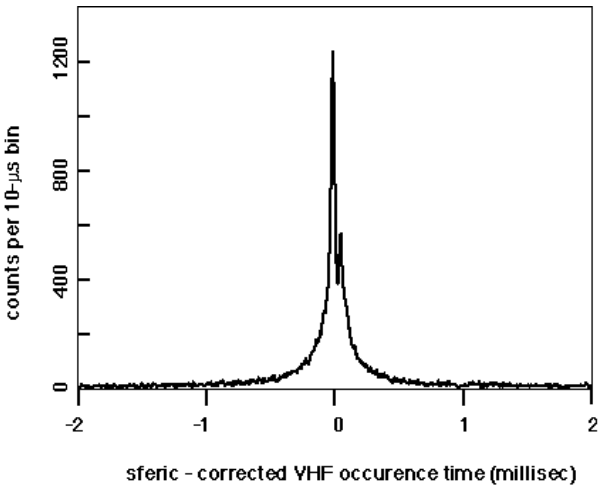

Implementation of the propagation corrections (above) leads to coincidence lags on the order of 100 μs, so we need to be more selective about the VHF events that we include. The VHF recorded event record is typically 400 μs in duration, and typically the record contains 100 μs of pretrigger samples plus 300 μs of posttrigger samples. If the pulse is narrow (see, for example, Plate 1 above, in which the event duration after postprocessing is <10 μs), then the power in the dechirped VHF is localized to the trigger time to within 10 μs, and it is meaninful to attempt to elucidate the NLDN-FORTE coincidence relationship to a finer scale than 100 μs. On the other hand, if the VHF event is not a narrow pulse compared to the desired coincidence resolution, but rather has energy distributed over several tens of μs on either side of the trigger time, then the FORTE timestamp cannot be meaningfully specified to any finer level than several tens of μs. Therefore it makes sense to limit the next step to include only those FORTE VHF events whose power 1/e width [*Jacobson et al.*, 1999] is <10 μs.

Figure 5 shows the histogram of NLDN-FORTE timestamp differences, now in the reduced range of -0.6 ms to +0.6 ms, again with a 10-μs bin size, restricting FORTE

events to those whose power 1/e width is <10 μs. Now we see that the main NLDN-FORTE coincidence peak occurs at -10 μs to -20 μs, that is, for *the VHF emission occurring after the LF/VLF emission*, by a lag of 10 μs to 20 μs. We also see that the overall coincidence above the accidental floor, including the secondary peak and the skirts of the distribution, is *entirely contained* within ±0.3 ms. Finally, the central-peak fullwidth at half-max is only ~30 μs.

Figure 5: Similar to Figure 4, but limited to FORTÉ VHF pulses with width <10 μs, and further zoomed-in, to ±0.6 ms.

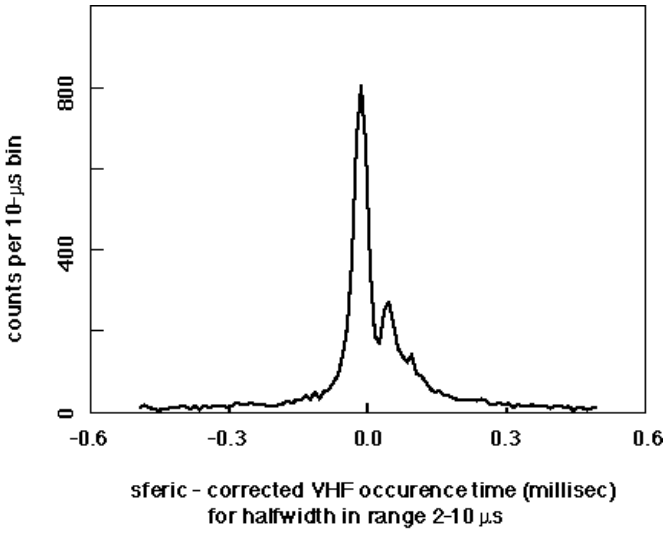

4. (b) Identification of VHF event with class of lightning discharge

At this point, we divide the VHF events according to what class of lightning discharge that they are coincident with. The choice of class is: positive cloud-to-ground ("+G"), negative cloud-to-ground ("-G"), intracloud ("C"), and untyped ("0"). The untyped ligntning discharges, as discussed in Section 3 above, are those that occur >600 km from the nearest NLDN station participating in the detection/geolocation. There is additionally some possible contamination of the positive cloud-to-ground class with LF/VLF signature s which actually arise from intracloud discharges (see Section 3 above).

Figure 6 shows the innermost coincidence distribution, from -0.2 ms to +0.2 ms, with a 10-μs bin size, for each class of coincident lightning discharge, again restricting the VHF

events to 1/e width <10 μs. Evidently the secondary peak is entirely due to the "0" events. As explained in Section 3 above, their LF/VLF timestamps had been expected to be ~several tens of μs late (relative to ground wave), due to ionospheric propagation effects. Otherwise, the primary peak is mainly due to the sum of (a) both polarities of cloud-to-ground strokes and (b) the intracloud strokes.

Figure 6: Similar to Figure 5, but subdivided into class of associated discharge, and further zoomed-in, to ±0.2 ms.

On the basis of our findings on a prompt -coincidence peak, we will now accept as "valid coincidences" all those for which the NLDN-FORTE timestamp lag is in the range -0.3 to +0.3 ms. This criterion results in only 14,985 valid coincidences over the entire six-month campaign. This means we have 14,985 FORTE events that we believe we can geolocate on the basis of their NLDN coincidence.

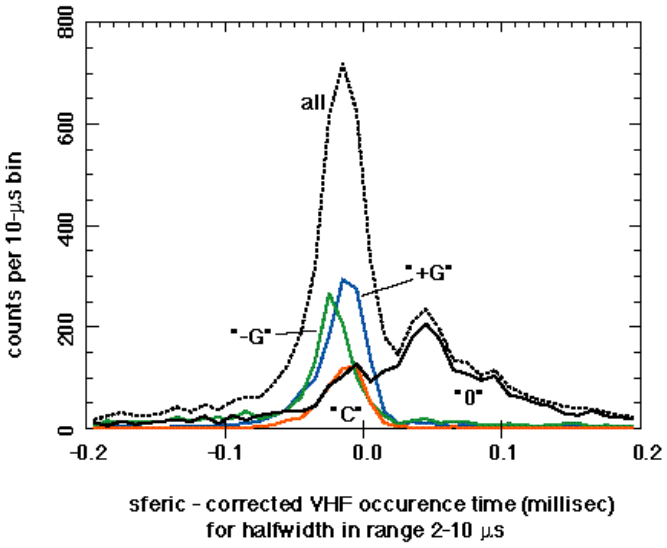

What is the expected contamination from accidental coincidences? We can estimate this by noting that outside the accepted range of range -0.3 to +0.3 ms, there remains a flat floor in the distribution, covering a domain 400 ms (minus the 0.6 ms in the central coincidence zone), and containing 261,023 - 14,985 events. This implies an accidental-coincidence rate of 616 per ms, or an expected contamination (in the range -0.3 to +0.3 ms) of 369 accidental events. This contamination is only 2.5% of the 14,985 accepted events. This 2.5% should be borne in mind when we attempt to frame conclusions about a small minority of the accepted events based on their NLDN-furnished geolocations. We must

assume that no statistically valid conclusions can be drawn on subpopulations as small as a few percent of the overall 14,985 accepted population.

Figure 7: Histograms of FORTE elevation angle seen from source location, for all LF/VLF signatures within ±200 ms of a VHF event (background) in dashed curve, and for all LF/VLF signatures within ±0.3 ms of a VHF event (prompt coincidence) in solid curve.

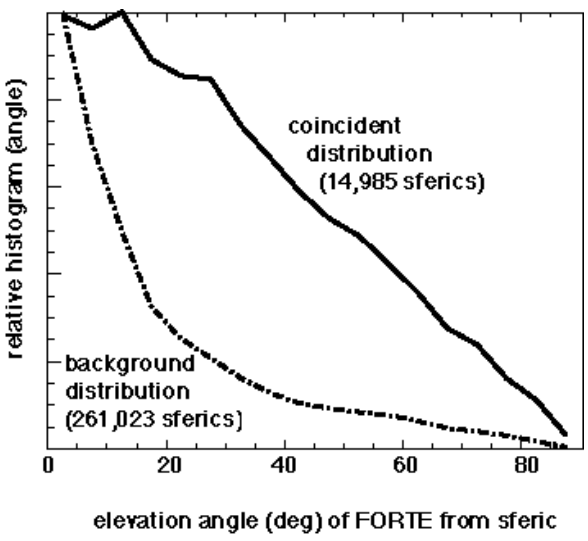

4. (c) Implied likelihood of intense VHF emissions from the lightning-discharge classes

Figure 7 shows histograms of the FORTE elevation angle relative to an Earth-based observer at all 261,023 lightning discharges (dashed curve) and only the accepted 14,985 lightning discharges (solid curve). The rise of the dashed curve at low elevation angle is due to the greater surfacearea contribution from the Earth's limb. The accepted events are far less likely to occur at the limb than are the overall population of candidate events. This is partly due to $1/r^2$ attenuation on the longer VHF pathlengths to the limb, and partly due to the antenna lobe of FORTE's primary antenna, which is directed toward nadir. Figure 8 shows the ratio of coincidences within the range -0.3 to +0.3 ms (known to be 97.5-% reliable coincidences), to those within -200 to +200 ms (known to be primarily accidental coincidences). This ratio, which we will call the "coincident:background ratio", or CBR, is due to a convolution of pathlength and the FORTE antenna directivity.

Figure 8: Ratio of the two curves in Figure 7, interpreted as being proportional to the efficiency of VHF detection versus FORTÉ elevation angle reckoned from the storm.

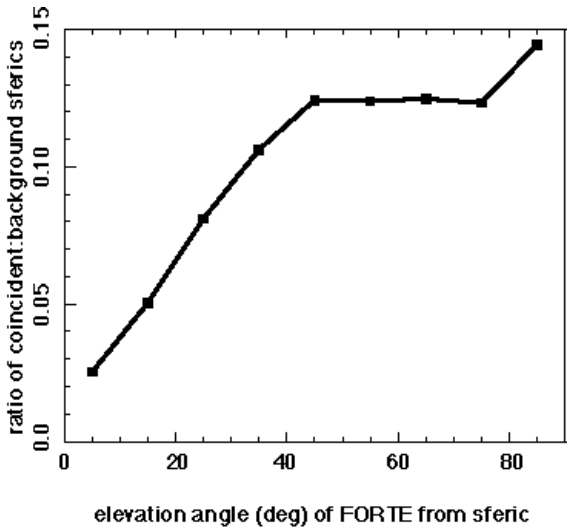

Figure 9 shows the CBR plotted against the lightning discharge's arcdistance (on the surface of the Earth) from the subsatellite point, separately for each lightning-discharge class. Each data point's arcdistance in Figure 9 is binned in annuli (on the Earth's surface) each of which contains $2X10^6$ km^2. The clear implication from Figure 9 is that intracloud discharges are ~10 times more likely to be accompanied by a detected FORTE VHF event than are negative cloud-to-ground lightning discharges, and that the positive cloud-to-ground discharges are ~5 times more likely to be accompanied by a detected FORTE VHF event than are negative cloud-to-ground lightning discharges. Part of this difference between the "+G" and "-G" classes may be caused by the possible contamination of the "+G" class by sferics arising from intracloud discharges (see Section 3 above).

The NLDN, like any ground-based LF/VLF array, is less efficient at detecting intracloud discharges than at detecting cloud-to-ground discharges . By contrast, the results in Figure 9 indicate that an intracloud discharge is much more likely to be accompanied by VHF strong enough to be detected by FORTE, than is a cloud-to-ground discharge. Thus there is a certain complementarity between the biases of NLDN and FORTE, resulting in there being rather few NLDN-FORTE coincidences, or equivalently, in the overall CBR being low.

Figure 9: Ratio of {LF/VLF signatures accompanied by prompt-coincident FORTE VHF event} to {all LF/VLF signatures within ±200 ms, including unaccompanied background LF/VLF signatures}, versus arcdistance (on surface of Earth) from subsatellite point to the source location. Each curve pertains to a different discharge class.

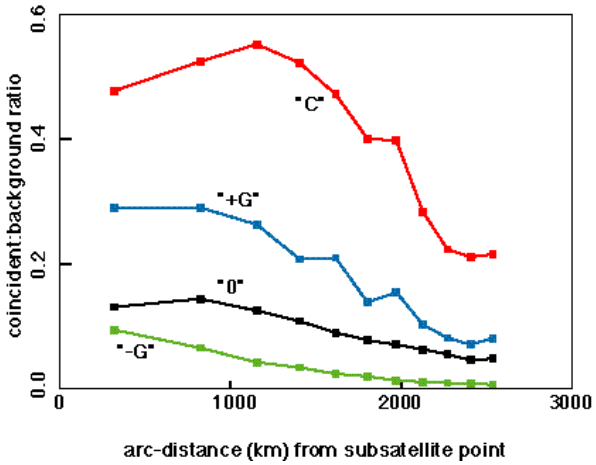

4. (d) Geographical distribution of coincident events

Atmospheric electricity during the April-September 1998 study period was affected early by anomalous El Nino storms in the SE CONUS and by regional smoke from Central American fires later in the Spring [*Lyons et al.*, 1998]. Plate 2 shows the location of the 14,985 FORTE events geolocated by NLDN coincidence in the range -0.3 to +0.3 ms. The class of the accompanying discharge is noted by color: black= "0", blue="+G", green="-G", and red="C". Note the prominence of maritime lightning (mostly in April and May) off the SE coast, and the paucity of "+G" associated events there. By contrast, the "+G" associated events are common over land, and the concentrations in the southern Great Plains were thought to be elevated during periods of invasive smoke from Central America [*Lyons et al.*, 1998]. The coastal nature of the coincidences near Mexico more or less reflects the NLDN background distribution for that region.

Plate 2: Location of the 14,985 sources which are accompanied by prompt-coincident FORTE VHF events. The class of the accompanying discharge is noted by color: black= "0", blue="+G", green="-G", and red="C".

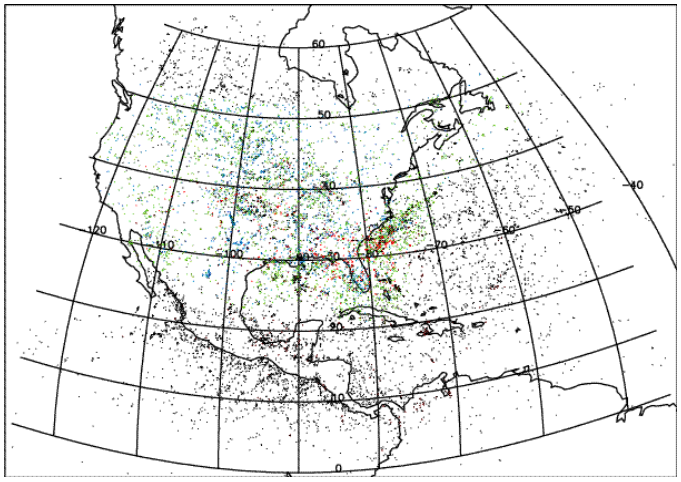

4. (e) Characteristics of VHF events geolocated by NLDN

As part of the data reduction for all events in the FORTE VHF archive, we compute and store the 1/e halfwidth of the autocorrelation function of the postwhitened, dechirped power [*Jacobson et al.*, 1999]. This is close to the pulse 1/e width in most cases. Figure 10 shows histograms of this measure of width, for VHF pulses accompanying all four classes of discharge. Although the paucity of "C" events makes the intracloud curve statistically meaningless at widths > 20 μs, nonetheless we can state that there is a qualitative difference between the VHF pulsewidths accompanying intracloud and cloud-to-ground discharges: The "C" VHF pulses are much more likely to be narrow (<10 μs) compared to the "+G" or "-G" pulses.

Figure 10: Histogram of power-correlation alf width for FORTE VHF pulses which are promptly coincident with a LF/VLF signature. Each curve pertains to a different accompanying discharge class. There are 7353 untyped ("0"), 2882 positive cloud-to-ground ("+G"), 4083 negative cloud-to-ground ("-G"), and 665 intracloud ("C") discharges.

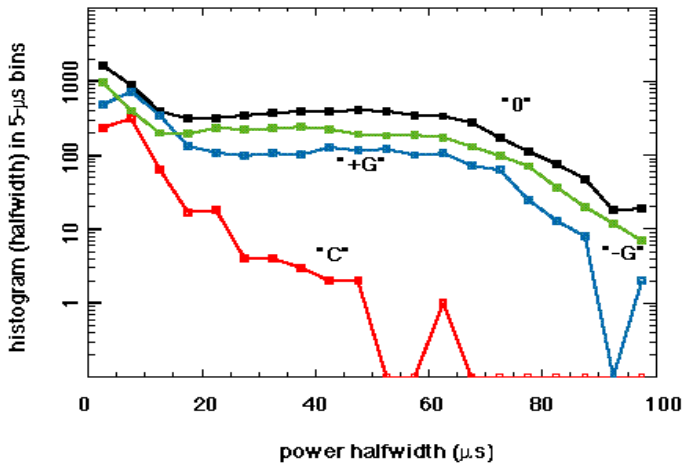

Figure 11 shows histograms of the log (base 10) of the peak source power at the VHF emission source, assuming isotropic VHF radiation, within the 22-MHz bandwidth

centered at 38 MHz. These distributions are obtained by converting the Poynting flux at FORTE to source power and assuming no attenuation. These distributions may understate the power by up to a factor of ~3, because they do not take account of the FORTE antenna lobe's attenuation off of nadir. Another factor of ~2 understatement may occur due to ionospheric D-layer absorption, at least for daytime events [*Budden*, 1988].

Figure 11: Histogram of logarithm of peak emitted power (in a 22-MHz band centered on 38 MHz) at the geolocated source, which is assumed to radiate isotropically. The estimate of power ignores the FORTE antenna's directional lobe. Each curve pertains to a different accompanying discharge class.

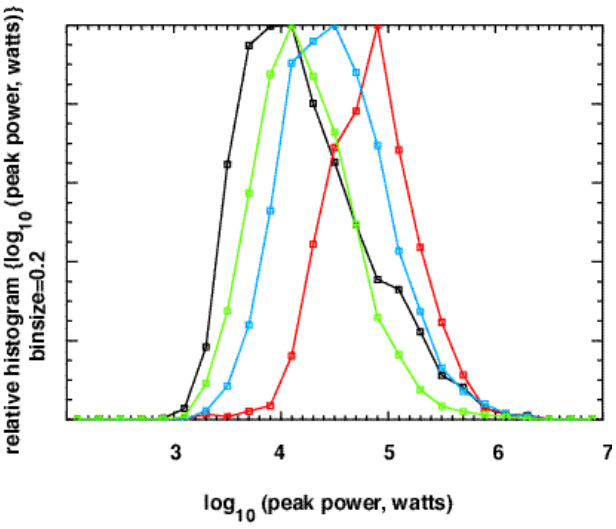

The obvious result in Figure 11 is that the peak powers in VHF pulses accompanying intracloud discharges are almost a factor of ~10 higher than the peak powers in VHF pulses accompanying negative cloud-to-ground discharges (which are the dominant contributor to the NLDN stroke archive.) Moreover, the positive cloud-to-ground discharges are accompanied by more intense VHF than are the negative cloud-to-ground discharges. Part of this difference between the "+G" and "-G" classes may be caused by the possible contamination of the "+G" class by sferics arising from intracloud discharges.

We reiterate that the fall-off of these curves toward the left, i.e. toward low power, may be substantially due to the FORTE trigger threshold. On the other hand, the fall-off of these curves toward the right, i.e. toward high power, is certainly due to the actual reduction in lightning emission rate versus power in that regime of powers.

We recall the example in Plate 1; that event was only 100 Watts/MHz at the source, or only 2.2 KW (in 22 MHz) on the abscissa of Figure 11. This makes the example of Plate 1 weaker than the peak of even the pulse distribution associated with negative-cloud-to-ground discharges.

Figure 12 shows histograms of the total energy emitted (assumed isotropic) in the FORTE VHF pulses, totaled over both time and the 22-MHz bandwidth centered on 38 MHz. Here the VHF pulse energies associated with intracloud and with positive cloud-to-ground discharges are virtually identical. The lower peak power (see Figure 11 above) of the events associated with positive cloud-to-ground discharges is compensated by those events' longer pulsewidths (see Figure 10 above). The peak of energies for these two energetic classes of events is at ~0.6 joules in 22 MHz, for a spectral density of .03 joules/Megahertz. This is comparable to the typical estimated energy density in the low VHF in TIPPs observed by Blackbeard [*Holden et al.*, 1995; *Massey and Holden*, 1995; *Massey et al.*, 1998].

Figure 12: Similar to Figure 11, but histogram of logarithm of total emitted energy .

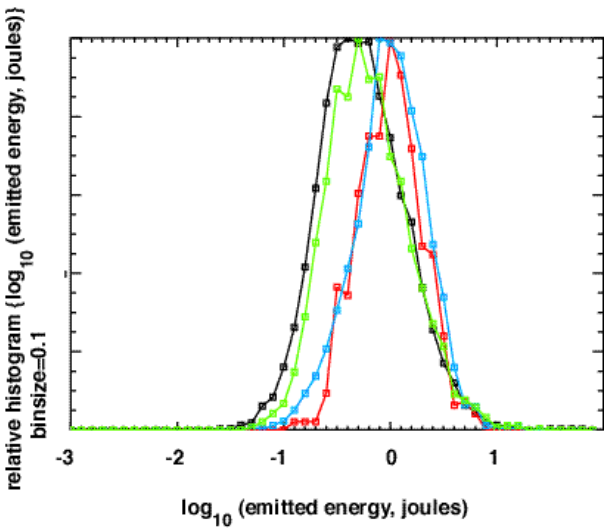

We caution that the North American sector, where this campaign's data were acquired, is the region on Earth with the highest level of anthropogenic radio noise, throughout much of the VHF. Thus our noise-riding trigger threshhold caused the effective absolute trigger levels to ride up for this study, compared to more radio-quiet parts of the Earth, including most equatorial zones. Therefore we can pose but not

currently answer the questions: If we had lightning-geolocation information in quieter areas (and we currently do not), would we find a FORTE event distribution extending lower (in both power and energy) than is the case in this CONUS study?

We reiterate that we must expect a stark contrast between satellite -measured lightning VHF and ground-sensor-measured lightning VHF. Satellites view a large area of the Earth's surface, see noise sources integrated over a huge area, and thus collect only very bright and energetic events compared to those collected by ground-based sensors, which see much less contributory noise background and thus can trigger on weaker emissions. This was indicated earlier with the Blackbeard observations [*Holden et al.*, 1995; *Massey and Holden*, 1995; *Massey et al*., 1998] and is both confirmed, and extended to a wider class of VHF waveforms, by FORTE.

Figure 13: Separately-normalized histograms of vertical-current amplitude in NLDN-detected lightning discharges. Solid curves: discharges which are prompt-coincident with FORTE VHF triggers; dotted curves: discharges which are not prompt-coincident. The number of discharges for each curve is noted next to the curve. (a) Intracloud, (b) negative cloud-to-ground, and (c) positive cloud-to-ground discharges.

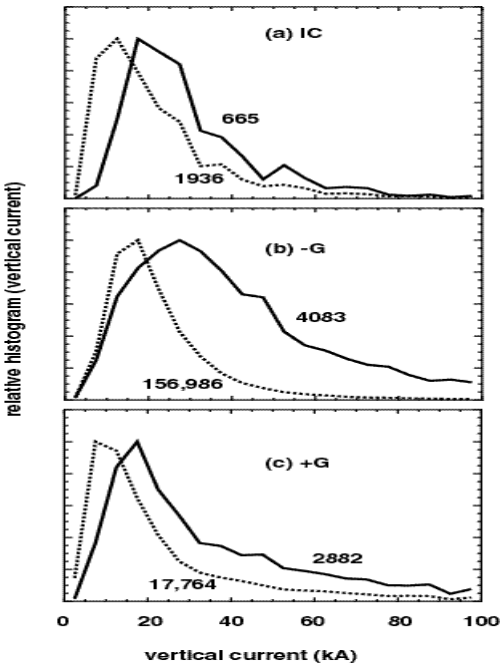

4. (f) Relationship between VHF pulses and lightning-discharge amplitude

The NLDN archive for this campaign contains a quarter-million discharges within ± 200 ms of a FORTE VHF event. Only ~15,000 of these discharges are convincingly (within ±0.3 ms) coincident with VHF events. Figure 13 shows histograms of equivalent-vertical-current magnitude from NLDN discharge reports. Each histogram is separately normalized, as we are

interested mainly in the histogram's shape. The "0" class is of course excluded, because current estimates for those long-range detections are not considered reliable (see Section 3 above) in terms of current. The solid curves in Figure 13 pertain to the FORTE-coincident discharges. The dotted curves pertain to the overall quarter-million discharges (minus the "0" class). Clearly the lightning discharges which are coincident with FORTE VHF triggers systematically tend to be higher-current than are the overall background of discharges. It appears that large-current discharges are more likely to be accompanied by prompt-coincident VHF at a level that is observable by FORTE.

Figure 14: Ratio of prompt-coincident lightning discharges (within±0.3 ms of a FORTE trigger), compared to all lightning discharges within ±200 ms of a FORTE trigger, in each of twenty current amplitude bins of width 5 kA. (a) Intracloud, (b) negative cloud-to-ground, and (c) positive cloud-to-ground discharges.

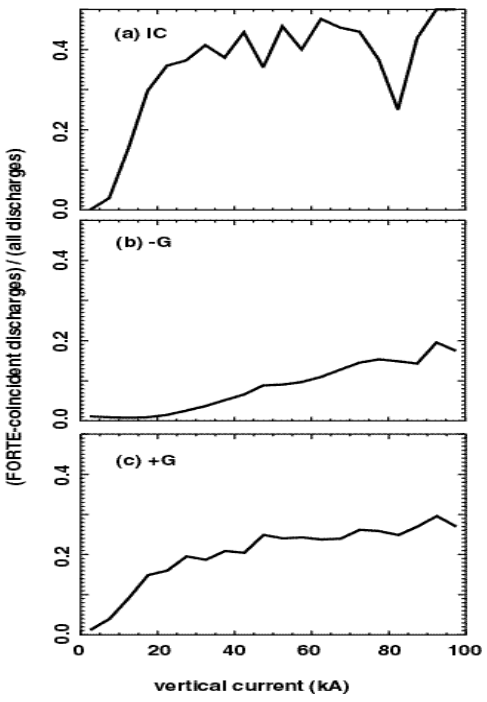

Figure 14 shows the ratio of prompt-coincident lightning discharges to all lightning discharges, in 5-kA bins of equivalent-vertical-current amplitude . This may be regarded as an experimental probability of seeing a VHF trigger with FORTE, given an NLDN-detected sferic from that discharge, versus the vertical current amplitude of that discharge. For all three classes of discharges, the probability of a VHF trigger drops dramatically for low-current discharges. The few "IC" discharges in the archive tend to produce the same VHF-detection probability for all but the lowest currents. "-G" discharges have a lower probability of being accompanied by VHF, but that probability rises versus discharge current amplitude without apparent saturation. "+G" discharges display a dependence of VHF-trigger

probability rises versus discharge current amplitude that is midway between these extremes.

Figure 15: Bar-chart of the logarithm (base 10) of the median total VHF source energy versus lightning-discharge current amplitude, in four 20-kA bins. a) Intracloud, (b) negative cloud-to-ground, and (c) positive cloud-to-ground discharges.

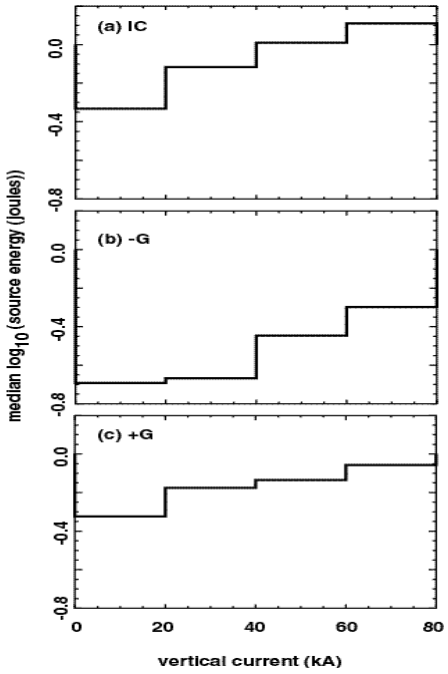

The discharge-current enhancement of the VHF-trigger probability raises the possibility that higher-current discharges tend to be accompanied by higher-energy prompt-coincident VHF pulses. Figure 15 shows a bar-chart of the logarithm (base 10) of the median total VHF source energy versus lightning-discharge current amplitude, in four 20-kA bins. There is a modest increase of VHF energy (by a factor of ~2), across the range of discharge current amplitudes. Thus, not only are VHF events more likely to accompany high-current lightning discharges (Figures 13 and 14), but the energy of the VHF emissions promptly coincident with high-current lightning discharges tends to be somewhat higher. In view of the fundamentally different emission mechanisms for LF/VLF and VHF radiated signals, our observational results in Figures 13-15 are not entirely expected. (We have also examined a scatter plot of individual events' rf energy versus NLDN-furnished vertical current. The scatter plot reveals far more variability than is indicated by Figure 15. Vertical current has skill at predicting ensemble-median rf energy in prompt-coincident rf pulses, but not at predicting individual rf pulses' individual energy.)

5. Ground-reflected pulses

It was suggested on the basis of Blackbeard observations [*Massey et al.*, 1998; *Smith*, 1998], and confirmed with FORTE [*Jacobson et al.*, 1999], that the second pulse in a TIPP is due to a ground reflection. This opens the possibility of inferring the emission height (above the reflecting ground) using the time-separation between the two pulses and the NLDN-furnished geolocation of the associated stroke.

Plate 3: Upper panel: Location of the LF/VLF signatures accompanying 2394 promptly coincident TIPPs. The class of the accompanying discharge is noted by color: black= "0", blue="+G", green="-G", and red="C". Lower panel:Same location as in upper panel, but with color indicating the retrieved height (above ground) of the TIPP emission region.

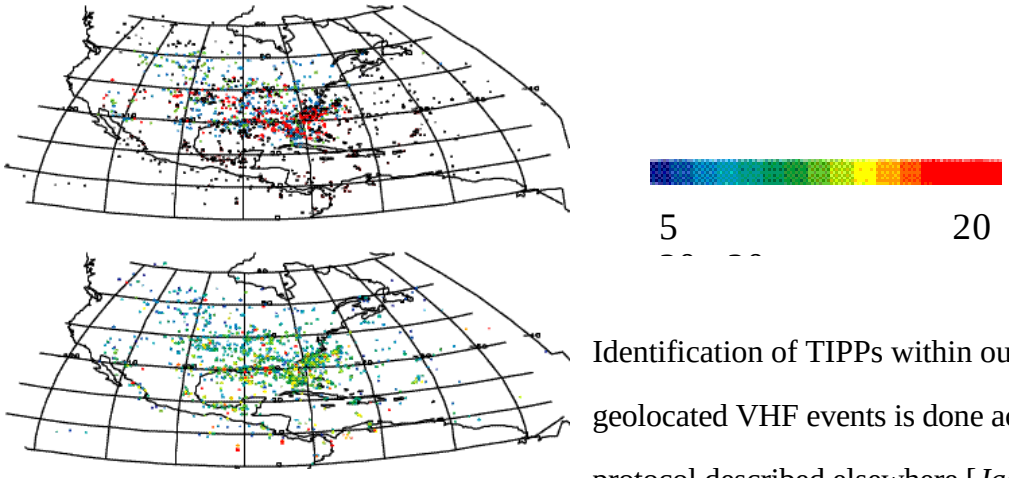

Identification of TIPPs within our 14,985 geolocated VHF events is done according to a protocol described elsewhere [*Jacobson et al.*, 1999], and we get in this manner 2394 TIPPs which are geolocated. We do not mean by the acronym "TIPP" to imply any special properties other than a pair of relatively narrow (<10 μs) pulses. The upper panel in Plate 3 shows the location of these 2394 TIPPs. The class of the accompanying discharge is noted by color: black= "0", blue="+G", green="-G", and red="C". It is interesting to compare these TIPP locations and discharge-class associations with the overall locations and discharge classes seen earlier (Plate 2). We observe that TIPPs are preferentially associated with intracloud discharges (when they are associated with a discharge at all). This is reasonable, in view

of the fact that TIPPs are more likely to be resolvable when the interpulse separation is large; originating as high as possible above ground increases the interpulse separation. Of the two polarities of cloud-to-ground discharges, we observe that negative cloud-to-ground discharges are especially *unlikely* to be associated with a TIPP. Part of this difference between the "+G" and "-G" classes may be caused by the possible contamination of the "+G" class by sferics arising from intracloud discharges. We also observe that the majority of our TIPPs were located in the southern maritime sector.

The lower panel of Plate 3 color-codes the inferred TIPP-emission height [*Jacobson et al.*, 1999] in the range 5 km (deep blue) to 20 km (deep red). We can see that all but a handful of these geolocated TIPPs originate below 20-km height (above ground), and that most originate below 15 km. This height distribution is consistent with the observed locus of rf emissions being within the active convective region of storms as opposed to being located higher, e.g. in the upper stratosphere [*Lhermitte and Krehbiel*, 1979; *Mazur et al.*, 1984; *Mazur et al.*, 1997; *Rhodes et al.*, 1994; *Shao et al*., 1996; *Shao and Krehbiel*, 1996; *Shao et al*., 1995; *Taylor*, 1978].

Another observation from the lower panel of Plate 3 is that there is a pronounced difference between emission heights in the northern/continental interior and emission heights in the southern maritime zones. We make this more quantitative in Figure 16, which displays histograms of the emission heights in two latitude/longitude rectangles: The dotted curve ("northern") lies within 65 < lat < 45 deg N and within -125 < lon < -50 deg E. The solid curve ("southern/maritime") lies within 10 < lat < 35 deg N and within -100 < lon < -60 deg E. Figure 16 indicates the dramatic height difference between these regions, a height difference that is broadly consistent with the inter-regional height differences of a given isotherm (e.g., -20 C) relevant to cloud electrification and discharge [*Lhermitte and*

Krehbiel, 1979; *Stolzenburg et al.*, 1998a; *Stolzenburg et al.*, 1998b; *Stolzenburg et al.*, 1998c].

Figure 16: Histogram of retrieved height (above ground) of the TIPP emission, in two latitude/longitude rectangles: The dotted curve ("northern") lies within 65 < lat < 45 deg N and within -125 < lon < -50 deg E. The solid curve ("southern/maritime") lies within 10 < lat < 35 deg N and within -100 < lon < -60 deg E.

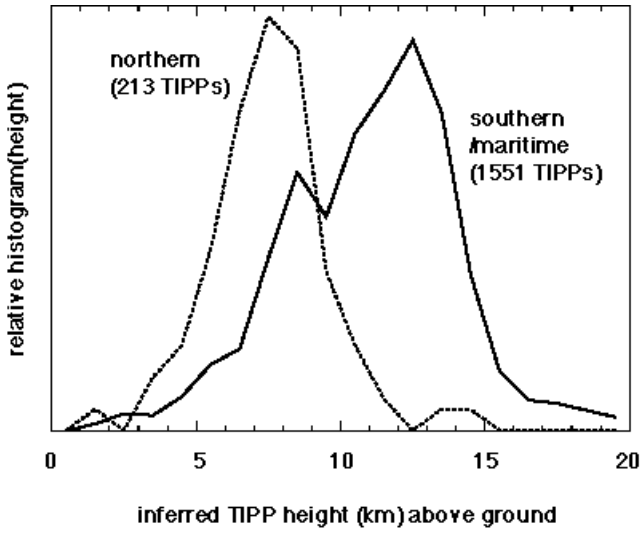

Still a third observation from Figure 16 is that there are a small number (on the order of 2%) of TIPPs above 15 km. However, in view of the similarity of this TIPP subpopulation's percentage to that of the estimated accidental-coincidence rate, we cannot necessarily treat this tail of very-high TIPPs with credence. They may be due simply to mistaken geolocation, which has a bias (given the huge field of view) of putting the event at an artificially distant location. This causes mistaken locations to tend to be biased toward *overly-high* height estimates [*Jacobson et al.*, 1999].

We have examined whether the inferred emission height is correlated with coincidence delay between the sferic and the VHF timestamps. We find no such correlation. We have also examined whether the inferred TIPP-emission height is correlated with the associated discharge vertical current as reported by NLDN. It is not.

6. Conclusions

(a) NLDN-FORTE coincidences which rise above the accidental coincidence level are prompt within ~30 μs, except for the NLDN strokes which are further than 600 km from the nearest participating NLDN sensor.

(b) FORTE-observed VHF emissions in the North America sector are often as strong as, or stronger than, Blackbeard-observed TIPPs.

(c) Satellite-observed VHF emissions are much more likely to be associated with intracloud discharges than with cloud-to-ground discharges. Satellite-observed VHF emissions are more likely to be associated with positive- than with negative-cloud-to-ground discharges.

(d) Satellite-observed VHF emissions associated with intracloud discharges tend to be narrower in pulsewidth than are VHF emissions associated with either polarity of cloud-to-ground discharges.

(e) TIPPs that are associated with NLDN discharges are even more likely to be associated with intracloud discharges.

(f) TIPPs that are associated with NLDN discharges display a region-dependent emission-height distribution, suggestive of the height-versus-latitude of key isotherms, e.g. -20 C, in the troposphere. Over the CONUS/Canadian interior above 45 deg N, the half-points of the distribution are at roughly 6 and 9 km, and the peak is at 7-8 km. Over the southern maritime region, the peak is at >13 km, and the distribution is broader. We have no statistically significant evidence, amongst the TIPPs that are associated with NLDN discharges, for TIPP-emission heights above 15 km.

Acknowledgement

This work was performed under the auspices of the United States Department of Energy.

References

Budden, K.G., *The Propagation of Radio Waves*, 667 pp., Cambridge University Press, Cambridge, 1988.

Cummins, K.L., M.J. Murphy, E.A. Bardo, W.L. Hiscox, R. Pyle, and A.E. Pifer, Combined TOA/MDF technology upgrade of U. S. National Lightning Detection Network, *J. Geophys. Res., 103* (D8), 9035-9044, 1998.

Hayenga, C.O., and J.W. Warwick, Two-dimensional interferometric positions of VHF lightning sources, *J. Geophys. Res., 86* (C8), 7451-7462, 1981.

Holden, D.N., C.P. Munson, and J.C. Devenport, Satellite observations of transionospheric pulse pairs, *Geophys. Res. Lett., 22* (8), 889-892, 1995.

Idone, V.P., D.A. Davis, P.K. Moore, Y. Wang, R.W. Henderson, M. Ries, and P.F. Jamason, Performance evaluation of the U. S. National Lightning Detection Network in eastern New York 1. Detection efficiency, *J. Geophys. Res., 103* (D8), 9045-9055, 1998a.

Idone, V.P., D.A. Davis, P.K. Moore, Y. Wang, R.W. Henderson, M. Ries, and P.F. Jamason, Performance evaluation of the U. S. National Lightning Detection Network in eastern New York 2. Location accuracy, *J. Geophys. Res., 103* (D8), 9057-9069, 1998b.

Jacobson, A.R., S.O. Knox, R. Franz, and D.C. Enemark, FORTE observations of lightning radio-frequency signatures: Capabilities and basic results, *Radio Sci.*, *34* (2), 337-354, 1999.

Le Vine, D.M., Sources of the strongest rf radiation from lightning, *J. Geophys. Res.*, *85* (C7), 4091-4095, 1980.

Lhermitte, R., and P.R. Krehbiel, Doppler radar and radio observations of thunderstorms, *IEEE Trans. Geosci. Electron.*, *GE-17* (4), 162-171, 1979.

Lyons, W.A., T.E. Nelson, E.R. Williams, J.A. Cramer, and T.R. Turner, Enhanced positive cloud-to-ground lightning in thunderstorms ingesting smoke from fires, *Science, 282* (2 October 1998), 77-80, 1998.

Massey, R.S., and D.N. Holden, Phenomenology of transionospheric pulse pairs, *Radio Sci.*, *30* (5), 1645-1659, 1995.

Massey, R.S., D.N. Holden, and X.-M. Shao, Phenomenology of trans-ionospheric pulse pairs, *Radio Science, submitted,* 1998.

Mazur, V., J.C. Gerlach, and D.W. Rust, Lightning flash density versus altitude and storm structure from observations with UHF- and S-band radars, *Geophys. Res. Lett.*, *11* (1), 61-64, 1984.

Mazur, V., E. Williams, R. Boldi, L. Maier, and D.E. Proctor, Initial comparison of lightning mapping with operational Time-of-Arrival and Interferometric systems, *J. Geophys. Res.*, *102* (D10), 11,071-11,085, 1997.

Proctor, D.E., VHF radio pictures of cloud flashes, *J. Geophys. Res., 86* (C5), 4041-4071, 1981.

Proctor, D.E., R. Uytenbogaardt, and B.M. Meredith, VHF radio pictures of lightning flashes to ground, *J. Geophys. Res., 93* (D10), 12,683-12,727, 1988.

Rhodes, C.T., X.M. Shao, P.R. Krehbiel, R.J. Thomas, and C.O. Hayenga, Observations of lightning phenomena using radio interferometry, *J. Geophys. Res., 99*, 13059-13082, 1994.

Roussel-Dupré, R., and A.V. Gurevich, On runaway breakdown and upward propagating discharges, *J. Geophys. Res., 101* (A2), 2297-2311, 1996.

Shao, X.M., D.N. Holden, and C.T. Rhodes, Broad band radio interferometry for lightning observations, *Geophys. Res. Lett., 23* (15), 1917-1920, 1996.

Shao, X.M., and P.R. Krehbiel, The spatial and temporal development of intracloud lightning, *J. Geophys. Res., 101* (D21), 26,641-26,668, 1996.

Shao, X.M., P.R. Krehbiel, R.J. Thomas, and W. Rison, Radio interferometric observations of cloud-to-ground lightning phenomena in Florida, *J. Geophys. Res., 100* (D2), 2,749-2,783, 1995.

Smith, D.A., Compact intracloud discharges, University of Colorado, Boulder, CO, 1998.

Smith, D.A., and D.N. Holden, Ground-based observations of subionospheric pulse pairs, *Radio Sci., 31* (3), 553-571, 1996.

Smith, D.A., X.M. Shao, D.N. Holden, C.T. Rhodes, M. Brook, P.R. Krehbiel, M. Stanley, W. Rison, and R.J. Thomas, Distinct, isolated thunderstorm radio emissions, *J. Geophys. Res., submitted,* 1998.

Stolzenburg, M., W.D. Rust, and T.C. Marshall, Electrical structure in thunderstorm convective regions 2. Isolated storms, *J. Geophys. Res., 103* (D12), 14,079-14,096, 1998a.

Stolzenburg, M., W.D. Rust, and T.C. Marshall, Electrical structure in thunderstorm convective regions 3. Synthesis, *J. Geophys. Res., 103* (D12), 14,097-14,108, 1998b.

Stolzenburg, M., W.D. Rust, B.F. Smull, and T.C. Marshall, Electrical structure in thunderstorm convective regions 1. Mesoscale convective systems, *J. Geophys. Res., 103* (D12), 14,059-14,078, 1998c.

Taylor, W.L., A VHF technique for space-time mapping of lightning discharge processes, *J. Geophys. Res., 83* (C7), 3575-3583, 1978.

Taylor, W.L., E.A. Brandes, W.D. Rust, and D.R. MacGorman, Lightning activity and severe storm structure, *Geophys. Res. Lett., 11* (5), 545-548, 1984.

Weidman, C.D., and E.P. Krider, The radiation field waveforms produced by intracloud lightning discharge processes, *J. Geophys. Res., 84,* 3159-3164, 1979.

Willett, J.C., J.C. Bailey, and E.P. Krider, A class of unusual lightning electric field waveforms with very strong high-frequency radiation, *J. Geophys. Res.*, *94* (D13), 16255-16267, 1989.

Zuelsdorf, R.S., C. Casler, R.J. Strangeway, C.T. Russell, and R.C. Franz, Ground detection of trans-ionospheric pulsed pairs by stations in the National Lightning Detection Network, *Geophys. Res. Lett.*, *25* (4), 481-484, 1998.

Zuelsdorf, R.S., R.J. Strangeway, C.T. Russell, C. Casler, H.J. Christian, and R.C. Franz, Transionospheric pulse pairs (TIPPs): Their geographic distributions and seasonal variations, *Geophys. Res. Lett.*, *24* (24), 3165-3168, 1997.